Platform for Model-Based Design and Testing for Deep Brain Stimulation

Ilija Jovanov,* Michael Naumann,* Karthik Kumaravelu,† Warren M. Grill† and Miroslav Pajic*
*Department of Electrical & Computer Engineering †Department of Biomedical Engineering
Duke University
{ilija.jovanov, michael.naumann, karthik.kumaravelu, warren.grill, miroslav.pajic}@duke.edu

***Abstract*—Deep Brain Stimulation (DBS) is effective at alleviating symptoms of neurological disorders such as Parkinson's disease. Yet, despite its safety-critical nature, there does not exist a platform for integrated design and testing of new algorithms or devices. Consequently, we introduce a model-based design framework for DBS controllers based on a physiologically relevant basal-ganglia model (BGM) that we capture as a network of nonlinear hybrid automata, synchronized via neural activation events. The BGM is parametrized by the number of neurons used to model each of the BG regions, which supports tradeoffs between fidelity and complexity of the model. Our hybrid-automata representation is exploited for design of software (Simulink) and hardware (FPGA) BGM platforms, with the latter enabling real-time model simulation and device testing. We demonstrate that the BGM platform is capable of generating physiologically relevant responses to DBS, and validate the BGM using a set of requirements obtained from existing work. We present the use of our framework for design and test of DBS controllers with varying levels of adaptation/feedback. Our evaluations are based on Quality-of-Control metrics that we introduce for runtime monitoring of DBS effectiveness.**

I. Introduction

Parkinson's disease (PD) is the second most prevalent neurological disorder [1], affecting nearly one million people in the US, with 60,000 new cases diagnosed every year [2]. With the aging population, which constitute the majority of patients suffering from the disease, the expectation is that these numbers will significantly increase. This will have a growing economic impact, as the US alone is estimated currently to spend $\$25$B annually for disease treatment, social security, and loss of income due to the inability to work, with PD patients spending $\$2,500$ – $\$100,000$ per year on treatment, depending on disease severity [2].

Deep brain stimulation (DBS) of the basal ganglia is effective even in the most severe cases of PD, and is also effective at treating symptoms of essential tremor and dystonia. Commercially-available DBS devices implement stimulation that is always 'ON', applying periodic pulses with fixed frequency and without any feedback from the patient (i.e., in open loop). Recently, it was shown that performance of DBS controllers can be optimized, both in open-loop and closed-loop setting, to increase the battery life of the implanted devices without compromising effectiveness of the therapy (e.g., [3]–[5]). Given research efforts focused on improving sensing technology for DBS, a rapid increase in the number of adaptive and closed-loop DBS devices is expected in the near future.

However, such devices will have significantly increased software design complexity, expected to exceed that of cardiac pacemakers and implantable defibrillators, which currently have 100,000 lines of code [6]. Even with existing, relatively simple controllers, there are a number of DBS device recalls due to software bugs; e.g., in 2013, more than 60,000 Medtronic DBS devices were recalled for software design [7]. With the increase in software complexity, these numbers will only rise, matching the trend for general medical device recalls where for instance, software failures resulted in 24% of all medical device recalls in 2011 [8], with more than 1,500,000 software-based medical devices recalled from 2002-2010 [9].

Although implantable medical devices, such as DBS devices, are a primary example of safety-critical Medical Cyber-Physical Systems, the medical device industry is only starting to use methods for development of safety-critical systems (e.g., [6], [10]), which were successfully employed in other domains (e.g., automotive, avionics). One of the main reasons is the lack of patient models and clinically-relevant simulators that can be used for both device design as well as safety and efficacy evaluation [6], [10]. For DBS devices, this is highlighted for closed-loop and adaptive DBS controllers; there is a need for high-fidelity, physiologically relevant models that can be used as part of an integrated development framework – both for model-based design and simulation-based evaluation of controllers, as well as for testing of their implementations (i.e., physical devices).

Although the underlying mechanisms of DBS are still not fully understood, there exist computational models of the basal ganglia (BG) in humans [11]–[13] and rats [14], which represent the response of neurons to DBS therapies. These models were employed to derive more efficient open-loop therapies based on the use of non-regular temporal patterns of stimulation that reduce energy consumption while lessening PD symptoms [3]. However, the high-computational complexity of such models results in 4 to 5 orders of magnitude increase in execution-time compared to real-time. This not only prevents their use for testing of physical devices, but also significantly limits their usability in development and evaluation of closed-loop and adaptive controllers. Thus, animal testing is still the dominant method for design and testing of DBS therapies (i.e., controllers).

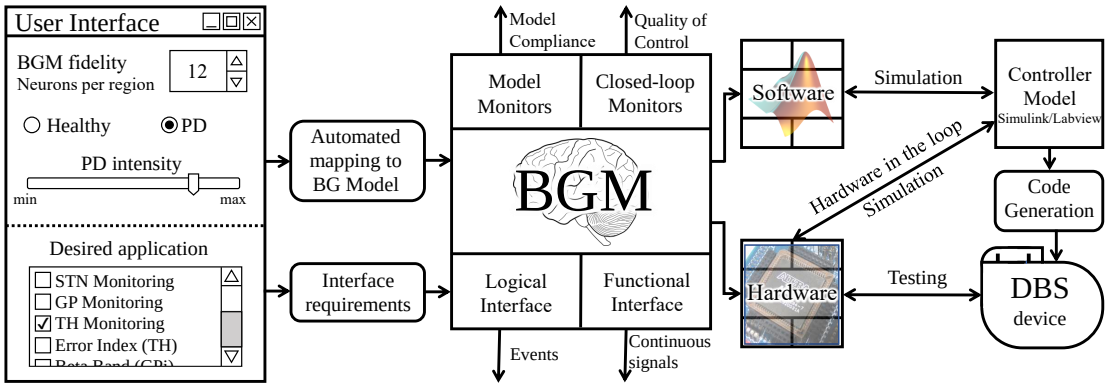

Figure 1. Model-based design framework for DBS devices – the developed BGM platform allows real-time physiologically relevant testing of DBS devices, as well as simulation of controller models in Simulink or LabView; simulations are done in real-time when hardware-in-the-loop (HIL) functionality is used.

We introduce a model-driven development framework for DBS controllers, illustrated in Fig. 1. First, we show that a physiologically relevant model of the basal ganglia can be captured as a network of nonlinear hybrid automata that synchronize via neural activation events – we refer to this model as the Basal Ganglia Model (BGM). The BGM is parametrized by the number of neurons used to model each of the BG regions, which supports tradeoffs between fidelity of representation and complexity of the model. From the network of hybrid automata models, software and hardware implementations of the BGM are obtained. Note that such a representation fits well with parallel execution models supported by FPGAs, and thus the hardware-implemented BGM platform capturing basal ganglia behaviors associated with both healthy and PD conditions, as well as the response to DBS, can be executed in real-time.

The platform also supports a fully programable interface enabling access to (a) functional (continuous) electrical potentials required for validation through simulation and device testing, and (b) logical signals that can be used for discrete-event based controller analysis. We provide a set of formal requirements for model validation and successful DBS control, and show how these can be checked at runtime by a suitable set of monitors. Finally, we show how the validated BGM model can be used for testing of DBS devices, as well as design and evaluation of existing and new controllers that optimize stimulation parameters, or employ adaptation of stimulation based on the patient condition.

This paper is organized as follows. In Section II, we provide more details on DBS. Section III introduces our BGM-based development framework. In Section IV, we describe the BGM and present formal requirements for model validation; this is followed by description of the BGM implementation. Section V shows the use of the BGM framework for DBS controller design and evaluation, before we provide concluding remarks in Section VI.

II. Deep Brain Stimulation

PD is a neurological disorder originating from degenerative changes in the substania nigra pars compacta (SNc) nucleus of the basal ganglia (BG) [1]. The disease manifests with multiple symptoms including tremor, slowed movement (bradykinesia), rigid muscles, impaired posture and balance, loss of automatic movements, and speech and writing changes. These symptoms are reflected in neural cell activity of surrounding regions, including globus pallidus interna (GPi) and thalamus (TH), where recordings can be conducted during implantation of DBS electrodes (Fig. 2). As illustrated in Fig. 3, healthy GPi and TH exhibit sporadic spiking (i.e., neuron activations) with an overall stable firing rate. On the other hand, in the PD state, GPi spiking becomes more frequent and grouped (burst-like), while TH signals exhibit burst activations and the inability to spike properly (i.e., reach activation/triggering levels).

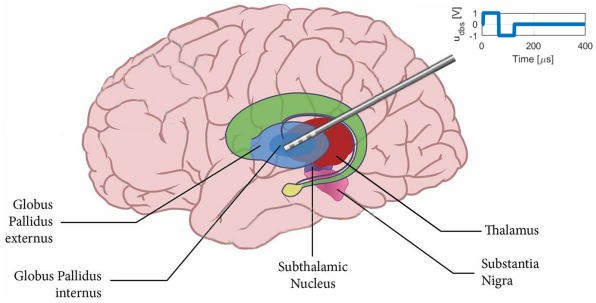

Figure 2. Location of different basal ganglia (BG) segments – we focus on the effects of DBS on the subthalamic nucleus (STN), globus pallidus externus (GPe), globus pallidus internus (GPi), and thalamus (THM). DBS electrodes (not to scale) are usually implanted in STN or GPi, delivering biphasic pulses. The figure is a modified version of [15].

High frequency (between 130 and 185 Hz) DBS of two BG segments – specifically, subthalamic nucleus (STN) and GPi – is effective in suppressing the major motor symptoms of PD. This is achieved by placing a thin metal 4-contact linear array electrode in the STN or GPi (Fig. 2). These leads generate a continuous train of short voltage pulses, with amplitude in the range of $[1, 3.5]$ V and duration between $60\mu s$ and $210\mu s$ for each phase of the biphasic pulse [16]. It is important to highlight that DBS increases the frequency of spiking in GPi (Fig. 3, right), which is not the same as the

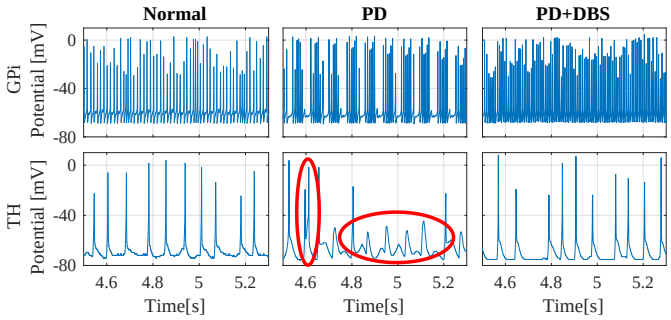

Figure 3. GPi and TH signals for healthy BG, parkinsonian BG, and parkinsonian BG treated with $130Hz$ DBS. Marked data shows aberrant Thalamus (TH) behavior – double activation and missed activation; with DBS, these behaviors subside.

expected behavior of GPi neurons in a healthy brain. Still, the therapy is effective since spiking is evenly distributed in GPi, and TH neurons recover their healthy behavior, showing alleviation of aberrant firing patterns seen in the PD state.

Existing DBS devices are delivering fixed parameter (voltage, pulse duration, pulse repetition frequency) stimulation constantly throughout the time they are deployed. This method of stimulation puts significant demand on the primary cell battery that powers the device, and requires surgical replacement every two to five years [17]. However, continuous stimulation is necessary as commercially available DBS devices have no sensing capabilities, and thus cannot detect when stimulation is required. To address this, recent research has focused on development of devices that enable both sensing and stimulation (although not at the same time instances), which would enable design of adaptive (closed-loop) DBS therapies [4], [5], [18]. Still, sensing limitations, including sensing technology and the number of BG points that can be monitored, prevent runtime controller adaptation, hence requiring medical staff to tune DBS parameters over several visits, which significantly increases the cost of the therapy. Even with multiple visits, due to the large number of potential stimulation parameters, selection of parameters that minimize PD symptoms remains challenging [16]. In addition, it is not possible to estimate how a specific parameter assignment would work for a specific patient prior to the surgery, and currently used testing procedures are based on device setting evaluation only after the device has been implanted.

III. DBS Development Framework

Fig. 1 illustrates our model-based framework for design and evaluation of DBS controllers. The framework is based on the BGM platform that supports both model-based and physical controller/device-based evaluations. Hence, the platform plays a crucial role during DBS device development by ensuring continuous controller validation, which directly enables implantable DBS device certification [19]. Starting from the controller modeling stage, the BGM can be used for virtual prototyping and controller development, by capturing desired physiologically-relevant patient conditions and interactions between the controller and BG neurons. That way any discrepancies between the control model and physical device implementation can be detected at an early stage.

Based on user requirements, the corresponding functional and logical interfaces of the BGM are generated. The logical (event-based) interface allows us to abstract the behavior of the BG regions as interaction of event-triggering nodes, which is a suitable level of abstraction for some DBS therapies; with such interface, discrete-event safety and efficacy analysis of the controller can be performed. On the other hand, the functional interface exposes the electrical potentials of the desired subset of BG neurons, thus enabling system analysis via simulation and testing of DBS devices.

The efficient, resource-aware implementation of the BGM as a network of non-linear hybrid-automata modeling basal ganglia neurons, allows us to model neuron interactions with the desired fidelity, by capturing dynamics of BG regions with a suitable number of neurons. This enables system designers to exploit tradeoffs between the BGM complexity and fidelity, as well as allow for execution of the BGM on resource constrained platforms (i.e., by using lower numbers of neurons). Note that as the number of modeled neurons changes, the behavior of the model can significantly change even though the rest of the BGM parameters remain the same. Thus, to ensure that a validated version of the BGM is used (for specific values of BGM parameters), we formally capture the requirements for model validation, and hence the platform automatically monitors whether the generated BGM configuration corresponds to a physiologically relevant basal-ganglia network. Similarly, our formalization of the level of success for the DBS therapy (i.e., controller) allows us to generate Quality-of-Control (QoC) runtime monitors that can automatically detect discrepancies between the desired QoC guarantees and the performance of controller/device at hand.

IV. Basal Ganglia Model of the Brain

In this section, we present the BGM, its hardware (in FPGA) and software (Simulink) implementations, as well as model validation based on a new formalized set of requirements for physiologically-relevant BG models.

A. Modeling Neural Activity

The overall structure of the model is shown in Fig. 4, with each of the components – thalamus (TH), subthalamic nucleus (STN), globus pallidus internus (GPi) and globus pallidus externus (GPe), capturing neural activity of the corresponding BG regions and their interaction. Note that although TH is technically not a part of BG, it reflects activity of GPi and helps with PD detection, and thus is included in the model.

Each component of the BGM is comprised of n neurons, with n being a design parameter, that are modeled using a variation of the Hodgkin-Huxley neuron model [20]

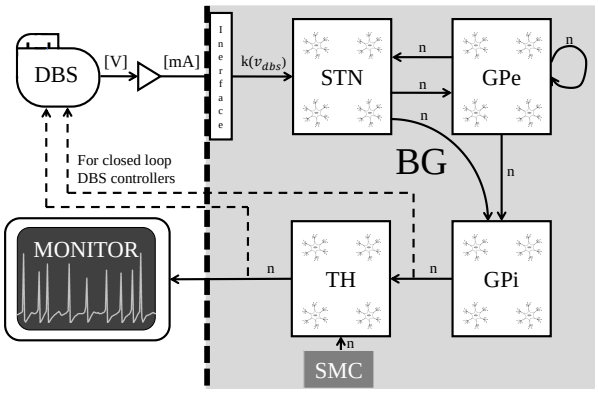

Figure 4. BGM network with components modeling the basal ganglia regions. The current stimuli from the DBS are delivered to a number (that depends on the DBS voltage levels) of STN neurons. Regions interact via neural activations that capture triggering of neurons in each BG region.

based on the region; thus, we name them after their origin (i.e., STN, GPe, GPi, TH). Activity of each neuron is mainly described by their *electrical potential*, which we denote by v_j^{TH}, v_j^{STN}, v_j^{GPi}, and v_j^{GPe}, for neuron $j \in \{1, ..., n\}$ of the corresponding region. Hence, the state of each BGM component can be captured with a *electrical potential vector*

$$\mathbf{v}^r = [v_1^r \dots v_n^r]^T \in \mathbb{R}^n, \quad r \in \{STN, GPe, GPi, TH\}. \tag{1}$$

The initial states of the neurons are one of the sources of stochasticity in the model, in addition to the sensorimotor cortex (SMC) current in TH (as described in the TH model).

Also, the neurons are interconnected through chemical synapses to form a BG network (Fig. 4). In general, these connections can be modeled as dynamical systems with impulse responses specified by the alpha synaptic function [14]

$$\alpha(t) = te^{\frac{-t}{\tau}}, \tag{2}$$

where parameter τ depends on the type of the synapse. However, to allow for discrete-event analysis of interactions between the brain regions in the BGM, we incorporate the synaptic functions into the neuron models specified as nonlinear hybrid automata; thus the inputs and outputs of the neurons are considered as discrete events, and interactions between the neurons are captured by event passing (i.e., synchronization) with neighboring neurons. We refer to these events as *neural activations*, and define them as follows:

Let $v_j^r(t) \in \mathbb{R}$, $r \in \{STN, GPe, GPi, TH\}$, $j \in \{1, ..., n\}$ represent electrical potential of the j^{th} BG neuron in region r, at time t. Then, the neuron generates a binary event a_j^r (i.e., a trigger) when $v_j^r(t)$ crosses over a predefined threshold h_j^r:

$$a_j^r(t) = 1 \Leftrightarrow (v_j^r(t) \geq h_j^r) \wedge (\exists \delta > 0, \forall \varepsilon \in (0, \delta], v_j^r(t-\varepsilon) < h_j^r). \tag{3}$$

We also define sets that capture activations originating from each neuron over time. Specifically, for j^{th} neuron in region r, we define the sets of all neural activations

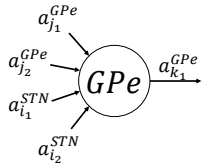

Figure 5. GPe neuron: Origins of receiving and destinations of transmitting events.

up to time t (denoted by $\mathcal{A}_j^r(t)$), as well as the set of all neural activations within the latest time-window of size T_w ($\mathcal{A}_{T_w,j}^r(t)$) as

$$\mathcal{A}_j^r(t) = \{t \mid (t' \leq t) \wedge (a_j^r \ triggers \ at \ t')\}, \tag{4}$$

$$\mathcal{A}_{T_w,j}^r(t) = \{t' \mid (t - T_w \leq t' \leq t) \wedge (a_j^r \ triggers \ at \ t')\} \tag{5}$$

For example, Fig. 5 illustrates one GPe neuron's connectivity with other neurons; the neuron receives events from two GPe and two STN neurons, while transmitting activations to connected neurons. In the rest of the section, we describe neuron models for each of the BG regions, focusing on the evolution of electric potential for different neuron types. The full set of model equations, based on dynamics from [11]–[13], is provided in the Appendix.

Subthalamic Nucleus: Each STN neuron receives events from two corresponding GPe neurons, as well as stimuli from the DBS device – the model of neural connectivity is presented in Section IV-A1. We also refer to the STN neurons as 'system input' neurons, as only they receive inputs from the controller. The electric potential evolution is described as [11]

$$\dot{v}^{STN} = \frac{1}{C_m}(i_{phys}^{STN}(v^{STN}) + I_{app} + i_{dbs} - i_{GPe \to STN}). \tag{6}$$

Here, i_{phys} comes from internal physiological processes of the neuron, I_{app}^{STN} is a constant current used to bias firing rates to physiological values, while i_{dbs} represents the current induced by the DBS; this current is usually set to $300\mu A/cm^2$ and follows the shape of DBS voltage signal. In addition, a higher DBS voltage input results in an increased number of excited neurons (as the stimuli reaches a larger number of neurons); thus, higher DBS amplitudes can be modeled by adding i_{dbs} to a larger number of STN neurons – i.e., by connecting them to the DBS as described in Section IV-A1.

Finally, let $\tau_{j_1}^{GPe}$ and $\tau_{j_2}^{GPe}$ denote the latest time of activations $a_{j_1}^{GPe}$ and $a_{j_2}^{GPe}$, originating from the connected GPe neurons and triggering the considered STN neuron. We can define the current caused by the events from GPe as

$$i_{GPe \to STN}(t) = g_{syn} S_{GPe,STN}(t)(v^{STN}(t) - E_{syn}), \tag{7}$$

where g_{syn} and E_{syn} are constants (see the appendix), and

$$S_{GPe,STN}(t) = \sum_{j \in \{j_1, j_2\}} \alpha(t - \tau_j^{GPe}).$$

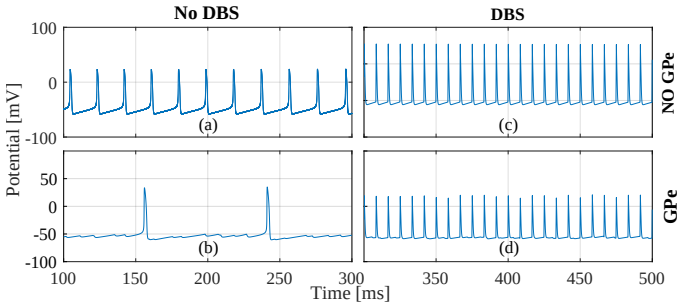

Figure 6. Evolution of electric potential in an STN neuron for several configurations – with and without DBS or events from neighboring GPe neurons; activations from the GPe have inhibitory effect on STN, while DBS overrides the intrinsic neural activations in the neuron with higher frequency stimuli.

From (2), $\alpha(t-\tau_j^{GPe})$, and thus $S_{GPe,STN}$ as well, re-initializes with every new activation of the GPe neurons.

Fig. 6 illustrates the dynamics of STN neurons. Without activations from neighboring GPe neurons or DBS inputs, the STN neuron electric potential is periodic, due to its internal dynamics (Fig. 6(a)). When we allow events from GPe to influence the STN neuron, the number of activations in STN decreases, showing inhibitory effects of GPe neurons (Fig. 6(b)). With DBS, external stimuli overrides the behavior of STN neurons unrelated to GPe activity (Fig. 6(c),(d)). This shows how DBS can regulate aberrant firing rate of STN caused by PD and other neurological disorders.

Globus Pallidus: Due to properties of neural cells in these regions, GPi and GPe electric potentials exhibit same dynamics. They provide intermediate processing between neurons in the STN that are directly excited by DBS ('input neurons') and neurons in TH where the effects of DBS are observed ('output neurons'); hence, they are sometimes considered a 'hidden layer' of the model. Still, GPi activity can be recorded for model validation, as it provides good insights into the inner workings of the BG regions.

GPi and GPe neurons receive four events (Fig. 5), from two STN neurons and from other two GPe neurons. They have one key difference – unlike the GPi, the GPe block effectively contains closed loops (i.e., cycles) due to interconnections between its neurons. Formally, dynamics of the electric potentials can be captured as (we use GP to denote either GPe or GPi)

$$\dot{v}^{GP} = \frac{1}{C_m}(i_{phys}^{GP}(v^{GP}) + I_{app}^{GP} - i_{STN\to GP} - i_{GPe\to GP}). \tag{8}$$

Again, let us define $\tau_{j_1}^{GPe}$ and $\tau_{j_2}^{GPe}$ as times of most recent activations in the GPe neurons that can trigger the considered GPe or GPi neuron. Then, we have that

$$\begin{aligned} i_{GPe\to GP}(t) &= g_{syn} S_{GPe,GP}(t)(v^{GP}(t) - E_{syn}), \\ S_{GPe,GP}(t) &= \sum_{j\in\{j_1,j_2\}} \alpha(t-\tau_j^{GPe}). \end{aligned} \tag{9}$$

Also, $i_{STN\to GP}(t) = g_{syn} S_{STN,GP}(t)(v^{GP}(t) - E_{syn})$, where, if i_1 and i_2 are the indices of the STN neurons connected to the considered GP neuron and $\mathcal{A}_{i_1}^{STN}$ and $\mathcal{A}_{i_2}^{STN}$ are defined as in (4), it holds that

$$S_{STN,GP}(t) = \sum_{t'\in\mathcal{A}_{i_1}^{STN}(t)} \alpha(t-t') + \sum_{t''\in\mathcal{A}_{i_2}^{STN}(t)} \alpha(t-t'').$$

Unlike re-initializing synaptic α function that was used for $S_{GPe,STN}$, due to its definition, $S_{STN,GP}$ will exhibit a cumulative behavior taking into account all previous activations, with larger impact coming from the more recent ones.

Thalamus: TH neurons receive one input from SMC and one event from GPi. As they generate no events for other neurons of BG, and their potential can be recorded to asses effectiveness of a DBS therapy, we also refer to them as monitor (i.e., sink) neurons. Their electrical potential is modeled as

$$\dot{v}^{TH} = \frac{1}{C_m}\left(i_{phys}^{TH}(v^{TH}) + i_{SMC} - i_{GPi\to TH}\right). \tag{10}$$

Here, current i_{phys}^{TH} comes from internal physiological processes occurring in TH (see Appendix), while i_{SMC} represents inputs from SMC. This current is modeled as a PWM signal with amplitude $3.5\mu A/cm^2$, pulse width of $5ms$, and inverse-gamma distributed random period with shape parameter 25 and scale parameter 1785.71. Finally, $i_{GPi\to TH}$ represents the effects of activations coming from the connected GPi neuron. Let $\mathcal{A}_j^{GPi}(t)$ denote the set of all activations from the GPi neuron, as in (4). Then, the resulting current can be modeled as

$$i_{GPi\to TH}(t) = g_{syn} S_{GPi,TH}(t)(v^{TH}(t) - E_{syn}), \tag{11}$$

with parameters g_{syn} and E_{syn} defined in the Appendix, and

$$S_{GPi,TH}(t) = \sum_{\forall t'\in\mathcal{A}^{GPi}(t)} \alpha(t-t').$$

1) Network of Neurons: The network of (i.e., signaling between) previously described neurons can be captured as a directed graph $(\mathcal{V},\mathcal{E})$, where $\mathcal{V} = \mathcal{V}^{TH}\cup\mathcal{V}^{STN}\cup\mathcal{V}^{GPe}\cup\mathcal{V}^{GPi}$ is the set of vertices capturing all n neurons in each of the modeled regions. The set of edges $\mathcal{E}$ is defined as

$$\begin{aligned} \mathcal{E} = &\left\{(v_j^{GPi}, v_j^{TH}) \mid 1\le j\le n\right\}\cup \\ &\cup\left\{(v_j^{GPe}, v_j^{STN})\right\}\cup\left\{(v_{j+_n1}^{GPe}, v_j^{STN}) \mid 1\le j\le n\right\} \\ &\cup\left\{(v_{j+_n1}^{GPe}, v_j^{GPi})\right\}\cup\left\{(v_{j-_n2}^{GPe}, v_j^{GPi}) \mid 1\le j\le n\right\} \\ &\cup\left\{(v_j^{STN}, v_j^{GPi})\right\}\cup\left\{(v_{j-_n1}^{STN}, v_j^{GPi}) \mid 1\le j\le n\right\} \\ &\cup\left\{(v_{j+_n1}^{GPe}, v_j^{GPe})\right\}\cup\left\{(v_{j-_n2}^{GPe}, v_j^{GPe}) \mid 1\le j\le n\right\} \\ &\cup\left\{(v_j^{STN}, v_j^{GPe})\right\}\cup\left\{(v_{j-_n1}^{STN}, v_j^{GPe}) \mid 1\le j\le n\right\} \\ &\cup\left\{(v_j^{DBS}, v_j^{STN}) \mid 1\le j\le \lfloor nu_{dbs}/u_{max}+0.2\rfloor\right\} \end{aligned} \tag{12}$$

where "$+_n$" and "$-_n$" denote addition and subtraction *modulo* n, while u_{dbs} and u_{max} denote current and maximal voltage of the DBS device, respectively. For example, the

connection from neuron v_j^{GPi} to neuron v_j^{TH} is captured by the first subset above.[1] Finally, each neuron can only receive events coming from *distinct* neurons, which is violated in (12) for $n = 1$ and $n = 3$. Thus, to obtain a valid BGM network, the lowest number of neurons per region is four.

B. Model Implementation

The Basal Ganglia Model was implemented both in hardware (FPGA) and software (Simulink). The Simulink BGM with $n = 10$ neurons per region was 4 orders of magnitude slower on a 6$^{\text{th}}$ gen. 3.5 GHz Intel i7 CPU with 16GB of memory than the FPGA BGM capable of running in real-time. Thus, the Simulink implementation allows for model-based design and evaluation of DBS control protocols directly in Simulink, while the FPGA BGM platform enables testing of physical DBS devices in real-time. Also, with Hardware-in-the-Loop (HIL) support we directly interface, in real-time, signals from the BGM platform to control models designed in Simulink or LabView, as shown in Sec. V.

To ensure consistency between the FPGA and Simulink BGM implementations, we implemented a discretized model of the BGM from Section IV-A. As the BGM is modeled as a network of hybrid automata, the discretized model was obtained using Forward Euler Method, as in e.g., [21], with sampling period of 100 kHz.[2] Since the Simulink BGM implementation was straightforward, due to Simulink's support for modeling of hybrid systems, here we focus on the FPGA implementation of the BGM.

The FPGA implementation of the BGM is fully parametric – i.e., suitable VHDL code for a specific number of neurons per region n is automatically generated. Also, the fully programable interface exposes electric potentials and activation signals from the desired neurons, where the former are upsampled (while ensuring that no activations are lost) to the sampling frequency of the DBS controller or data logger.

Given that the BGM can be described as a network of hybrid automata communicating via discrete events, the parallel execution model intrinsic to FPGAs provides excellent support for real-time execution. However, the complexity of the BGM conflicts with our goal to obtain a resource efficient VHDL implementation. Thus, we had to address the following challenges. First, the BGM is described using a high number of nonlinear functions for each of the neurons. To avoid their exact computation in real-time (and minimize the number of used hardware multipliers), we opted for the use of Look-Up-Tables (LUTs). We were able to represent all the required functions using linear operations and 4 basis functions captured by the LUTs: $f(x) = \frac{x}{x+10}$, $f(x) = \frac{x}{x+15}$, $f(x) = e^x$ and $f(x) = \frac{1}{1+e^x}$. Also, to minimize

[1]We sometimes abuse the notation by using v_j^r, to denote both electric potential of the j^{th} neuron in region r as well as the neuron itself.

[2]Due to discretization, some of neuron activations may be delayed by approximately $10\mu s$. To show that this does not introduce invalid BG behaviors, in the next subsection, we present the BGM validation by focusing on the FPGA BGM implementation.

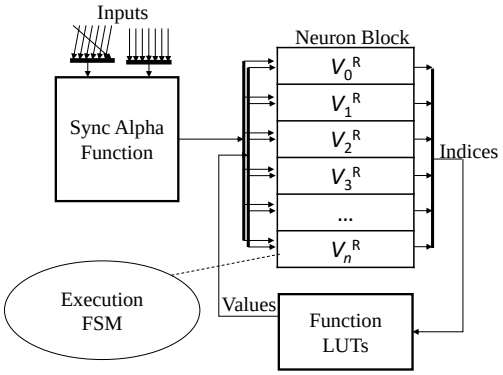

Figure 7. VHDL design architecture for each BG region – the execution FSM controls data flow and Look-up-Table (LUT) access within the neuron block; as all neurons in a region share the same execution Finite-State Machine (FSM), there are four total execution FSMs for the whole BGM. Finally, each of n neurons in a region is implemented using a separate 37 bit fixed-point multiplier implemented from four 18-bit multipliers.

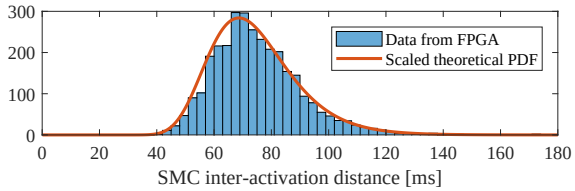

Figure 8. Histogram of (required and obtained) SMC inter-activation times.

memory use, the LUTs are shared between the neurons in each BG region. That on the other hand, introduced the problem of resource scheduling, requiring a design of an execution state machine (FSM) for each region, to control data flow between neurons and access to the LUTs (Fig. 7).

We also had to make a decision between fixed and floating point implementation, and the number of bits used for data representation. While floating point representation provides better precision, it requires far greater resources (logical elements and registers, fixed-point multipliers). Given that the BG behavior is quasi-periodic, we were able to account for a range of possible state values. Thus, to avoid potential overflow we opted for the use of 10 bits for the integer part. As most FPGAs provide 18-bit hardware multipliers, we support two implementations based on the use of 37-bit (obtained using four 18-bit multipliers) or 18-bit multipliers.

Finally, it is worth noting that suitable random generators are used for the SMC current (Fig. 8) and initial neuron states. We tested our design on Altera DE2-115 FPGA board (Fig. 12) that provided sufficient resources for $n = 10$ neurons per region, resulting in a model with good fidelity [3], [12], [14]. For an implementation based on the use of 37-bit multipliers, Table I provides a list of the required hardware resources for BGM with 10 neurons per region.

C. Model Validation

The fidelity of the BGM depends on the parameter settings and the number of neurons per region – we refer to these values as a *BGM configuration*. To validate the functionality

Resource	Used
Logic Elements	97,818
1-b Registers	54,604
HW Multipliers	320
Memory [b]	3,331,136

Table I
HARDWARE RESOURCE CONSUMPTION FOR THE BGM VHDL IMPLEMENTATION WITH $n = 10$ NEURONS PER BG REGION.

of the BGM, we compare behavior of the model to available recordings obtained from real patients with healthy and Parkinsonian brains, and show how the BGM can reproduce the underlying electrical activity of the BG regions.

Furthermore, we formalize a set of requirements that electrical activity in both the healthy and Parkinsonian states needs to satisfy. These requirements are captured using metrics that are defined over moving time-windows of suitable size, denoted by T_w; thus, we directly mapped them into a set of runtime monitors that can be used to validate if a specific BGM configuration captures the desired behaviors. Note that the specified set of constraints is used to capture behaviors without DBS – requirements for electrical activity of the BG under a successful DBS therapy will be described in Section V. Also, note that the Hodgkin-Huxley neuron model along with the α synaptic function results in a quasi-periodic behavior (as in Fig. 6). Therefore, although there is a great deal of variability in parameters between different subjects and electrode positions, for observation windows of suitable size, these metrics should remain consistent over time for any observed electrical activity in the BG regions.

1) Requirements and Metrics for Model Validation: To validate various BGM configurations, we employ the following set of metrics that capture regularity of specific events in the model. Based on experimental data available in literature, these metrics are then used to define a set of constraints that BGM signals capturing healthy and Parkinsonian behaviors should satisfy. It is important to highlight that some of these conditions may be satisfied for activations associated with both healthy and PD brains; e.g., the value ranges for mean firing rate metrics, defined below, as healthy and PD behaviors overlap for some BG regions. Hence, none of the constraints should be considered alone but rather all have to be satisfied for a model to pass validation. Also, the metrics are defined over the sets of neural activations during the last T_w time units (i.e., from (5)), with T_w being a design parameter. In our experiments, we used $T_w = 10\ s$ as in [14].

Mean Firing Rate (m^r_{fr}) within a region r (STN, GPi, or GPe) captures the average number of recorded activations originating from the region during the time-window – i.e.,

$$m^r_{fr} = \frac{\sum_{j=1}^{n} |\mathcal{A}^r_{T_w,j}|}{nT_w}, \quad r \in \{STN, GPe, GPi\}, \quad (13)$$

with $\mathcal{A}^r_{T_w,j}$ defined as in (5). *The mean firing rates of STN and GPi neurons are higher, whereas that of GPe neurons are lower for patients with PD compared to the healthy patients* (e.g., [22], [23]). Note that this test was originally developed for recordings from only the BG regions, and as such does not include TH. The left side of Table II presents experimental results available in literature (e.g., [23]).

Coefficient of Variation (C_v): GPi neurons in a healthy brain exhibit regular firing, while PD alters the dynamics to more irregular, burst-like activation patterns. This is captured by the coefficient of variation C_v for GPi neurons. To formally define C_v, we start from the set of inter-spiking-intervals (ISI) over time-window T_w as (for $j \in \{1, \ldots, n\}$)

$$\Theta_j(T_w) = \{\tau_{isi} = \tau_1 - \tau_2 \mid \tau_1, \tau_2 \in \mathcal{A}^{GPi}_{T_w,j} \wedge (\tau_1 < \tau_2) \wedge ((\tau_1, \tau_2) \cap \mathcal{A}^{GPi}_{T_w,j} = \emptyset)\},$$

where (τ_1, τ_2) denotes the open time interval between these points. Then, the Coefficient of Variation can be computed as

$$C_v = \frac{\sigma(\Theta_j(T_w))}{\mu(\Theta_j(T_w))}.$$

where σ and μ denote standard deviation and the mean value, respectively, across the elements of the set. *Coefficient C_v should be lower during the healthy condition compared to the PD state*. This characteristic was observed in experimental data from [24], and it also holds that in general $C_v \in [0.19, 0.82]$ for healthy brains, and $C_v \in [0.5, 0.97]$ for patients with PD, as shown in Table II.

Beta Band Power (P_β): Let $V^{GPi}_{T_w,j}(\omega)$ be the one-sided power spectrum of $v^{GPi}_j(t),\ j \in \{1, \ldots, n\}$, computed over the window T_w. As shown (e.g., in [14]), low-frequency oscillatory activity in the beta band (i.e., $[13 - 35Hz]$) is correlated to motor symptoms of PD. Hence, we compute parameter P_β as

$$P_\beta = \frac{1}{n} \sum_{j=1}^{n} \int_{\omega=2\pi \cdot 13Hz}^{2\pi \cdot 35Hz} V^{GPi}_{T_w,j}(\omega) d\omega.$$

If we denote the β-band power of a healthy and PD thalamus by P^h_β and P^{PD}_β, human and animal recordings have shown that P^{PD}_β has to be significantly higher than P^h_β – such as during episodes when a brain moves from exhibiting healthy behaviors to PD symptoms (e.g., if a drug is induced) [14]. Thus, for model validation, rather than inspecting the spectrum visually as is the common practice, *we consider the P^h_β / P^{PD}_β ratio, which should be lower than* 1 for valid BGM models.

2) Experimental Validation: We experimentally validated the BGM on several standard clinically relevant scenarios focused on behaviors associated with healthy and Parkinsonian brains. Using the hardware and software BGM platforms, we performed standard evaluation tests from [11], [12], [14]. Due to the space constraints, in this section, we show several common representations of the recorded data from GPi neurons only, for a BGM model with $n = 10$; specifically, we present time series, rastergram, and spectrum (Fig. 9), as well as ISI histogram (Fig. 10). As can be seen, time series from a GPi neuron show that GPi with PD has a higher

	Values from Literature		Developed BGM							
			$n=4$		$n=6$		$n=8$		$n=10$	
	Normal	PD	Normal	PD	Normal	PD	Normal	PD	Normal	PD
$m_{fr}^{STN}[Hz]$	$[9, 29]$	$[11, 41]$	11.68	13.52	10.08	12.59	10.14	11.34	10.34	12.66
$m_{fr}^{GPe}[Hz]$	$[47, 85.2]$	$[29.2, 67.8]$	70.08	40.56	70.6	37.77	71.48	31.73	70.16	37.99
$m_{fr}^{GPi}[Hz]$	$[59.8, 101.2]$	$[76.6, 135.4]$	78.69	81.14	72.11	88.16	76.62	91.28	74.23	82.86
C_v	$[0.19, 0.82]$	$[0.5, 0.97]$	0.247	0.627	0.203	0.74	0.205	0.47	0.202	0.65
P_β^h / P_β^{PD}	[0,1)		0.6613		0.7288		0.686		0.796	

Table II
COMPARISON BETWEEN AVAILABLE RESULTS IN THE LITERATURE AND THE RECORDED ACTIVITY FOR THE DEVELOPED BGM.

frequency with more bursty neural activations (Fig. 9(top)). The rastergram in Fig. 9(middle) and histogram in Fig. 10 further support this observation, showing that this holds for all neurons in the GPi of the parkinsonian BGM. Finally, a significant increase in power can be observed in the β-frequency band in the PD case.

Full comparison between experimental data obtained from literature and our implementation with $n = 10$ neurons is provided in Table II. While the obtained values lie within the required ranges, it can also be observed that all previously specified conditions are satisfied as well. For example, for all considered values of n, it holds that m_{fr} of STN and GPi are higher in PD compared to healthy BG, while the opposite holds for the GPe region. Furthermore, C_v is greater in the PD case, compared to the healthy BG. Note that although some values, such as m_{fr}^{STN} for $n = 4$ satisfy both healthy and PD requirements, when all constraints are taken into account none of the 'healthy' BGM models satisfied all (or even majority) of the PD requirements, and vice-versa. An interesting observation was that some metrics alone (e.g., m_{fr}^{GPe}) were shown as reliable features to (independently of others) differentiate between healthy and parkinsonian BG; investigating this further will be an avenue for future research.

In addition, as shown in Table II, the BGM remains valid for varying number of neurons ($n \geq 4$), both from the perspective of the required value ranges, as well as the described relationship between observed activations in Parkinsonian and healthy brains. This shows that the model can be implemented on even resource-constrained platforms. However, models with higher numbers of neurons still provide several advantages. First, the difference between parameters obtained for normal and PD conditions tends to increase with n, mainly for observed firing rates; given that synchronization of firing between different neuron groups is oftentimes increased in PD, a higher number of neurons n provides better model fidelity. In addition, a larger n allows more accurate modeling of the effects of DBS voltage modulation, such as changes in amplitude or shape (e.g., different types of biphasic voltage pulses).

V. MODEL-BASED DESIGN OF DBS CONTROLLERS

As part of DBS therapy, there are generally three parameters that can be changed – pulse width, frequency/temporal patterns, and voltage – with the goal of obtaining sufficient Quality of Control (QoC), while reducing energy consumption. In this section, we illustrate the use of our BGM platform for design and evaluation of DBS controllers and devices. We show how the BGM supports testing of existing DBS devices, as well as modeling and design of new controllers along with experimental evaluation once they are implemented. To facilitate this, we formalize the requirements for successful DBS, and implement them as runtime monitors providing real-time feedback about the QoC for the controller under consideration.

A. Quality of Control Metrics for DBS

Quality of control for a DBS controller is determined by PD symptoms. While symptom severity is usually diagnosed by a clinician that is observing patient's behavior, this test can be very subjective and inappropriate for automated QoC evaluation and parameter tuning. Hence, several metrics based on signals from TH and GPi are developed to evaluate severity of PD. Here, we consider two – Error Index (EI) [3], and Power Spectral Density (PSD) [14]. The definitions of the QoC metrics are based on the set of activations in a moving time-window of size T_w, which can be directly implemented as circular FIFO buffers of suitable size. Thus, without significant resource utilization, we included them into the BGM platform.

1) *Error Index (EI)* observes the number of healthy responses in TH to inputs from SMC – i.e., $EI(t) = \frac{N_{err}(t)}{N_{SMC}(t)}$. Here, N_{SMC} represents the total number of activations from the SMC inside the observed time window, i.e., $N_{SMC}(t) = |\mathcal{A}_{T_w}^{SMC}(t)|$ as defined in (5). Also, $N_{err}(t)$ tracks the number of *faulty TH activations* in relation to the received SMC inputs. Specifically, a TH activation is deemed faulty if TH neuron corresponding to an SMC input does not have exactly one activation inside the $25\ ms$ time-window following the SMC activation. The value EI equal to 0 is associated with no PD symptoms, while the EI value 1 represents the most severe case of PD.

2) *Power Spectral Density* (PSD) is computed over the β-band spectrum of signal inside of the time window T_w, since a healthy brain exhibits a consistent shape of PSD, while parkinsonism causes increased activity in the beta frequency range. Thus, we use P_β as in Section IV, where higher values of P_β indicate increased severity of PD symptoms.

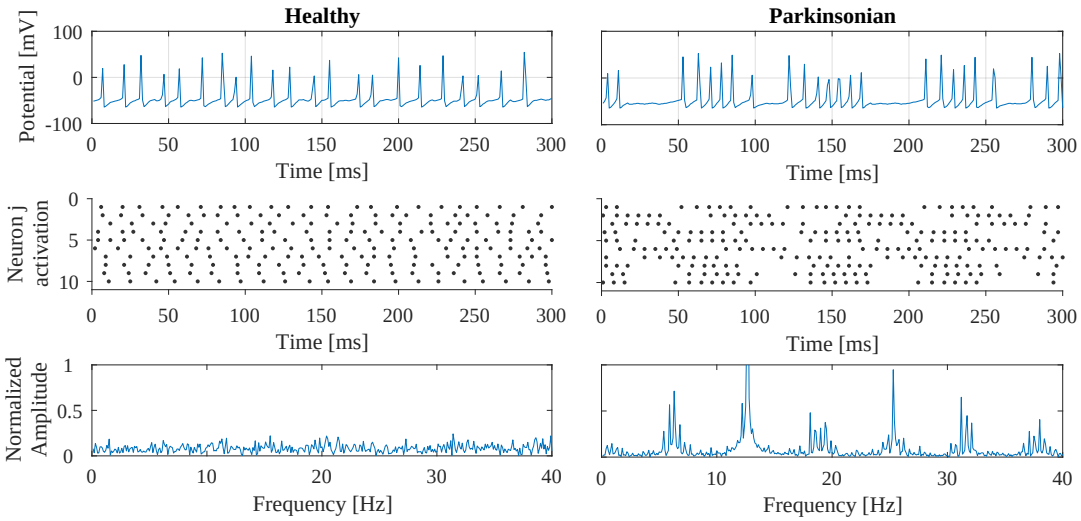

Figure 9. Time series of a single neuron, and rastergram and averaged normalized spectrum of all $n = 10$ recorded GPi neurons. The difference between parkinsonian and healthy BG is that PD neurons fire in bursts of more frequent activations, and β-band activity ($[13, 35]\ Hz$) is significantly increased.

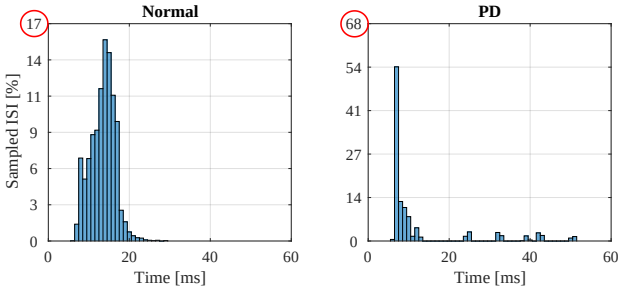

Figure 10. Histograms of inter-spiking intervals (ISI) of GPi neurons. In a healthy brain, activations arrive at variable time distances, grouped around the mean value. For PD brains, inter-spiking intervals are divided into more spaced bins of equidistant activations.

B. DBS Controller Design and Validation

To illustrate the use of the BGM-enabled design and evaluation framework, we considered three types of controllers: 1) Classic controller, denoted by $\mathcal{C}_{freq}$, is a conventional DBS device used in clinical practice. It continuously provides a periodic signal with amplitude equivalent to $300\mu A/cm^2$, pulse width of $300\mu s$ and pulse repetition frequency in the $130Hz - 180Hz$ range.
2) Pattern-based controller ($\mathcal{C}_{patt}$) is similar to the classic controller, as it persistently delivers pulsatile stimulation. This recently proposed type of controller [3] employs any temporal pattern with a constant firing rate over a large time window, instead of having constant frequency; reduction in energy consumption is achieved by the use of lower pulse repetition frequencies. The main challenge is to find a suitable temporal patternof stimulation [3].
3) Adaptive controller ($\mathcal{C}_{adapt}$) is based on the recently proposed sensing technology (though not deployed in practice). Given that the stimulation signal has significantly higher amplitude than the signal being recorded, sensing and DBS have to be done in separate time slots [18]. In our design, $\mathcal{C}_{adapt}$ periodically (every 10 s) measures GPi

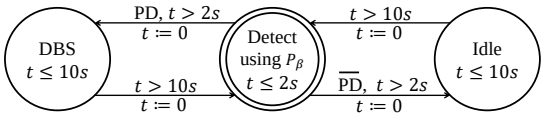

Figure 11. Adaptive controller $\mathcal{C}_{adapt}$ that periodically checks for presence of PD symptoms (using P_β values) and stimulates accordingly, thus increasing the battery lifetime of the device.

signal for $T_{sens} = 2s$, after which it decides whether to start stimulation or remain dormant for the following $10s$; the decision is based on the β-band power calculation (Fig. 11).

The aforementioned controllers were designed and tested using testbed shown in Fig. 12. Specifically, (a) $\mathcal{C}_{freq}$ was implemented directly in a Cortex-M3 microcontroller, (b) the exploration of temporal patterns for $\mathcal{C}_{patt}$, based on a search similar to the one from [3], was done in LabView using HIL real-time simulation support and directly employing the feedback from QoC monitors on the platform, and (c) for $\mathcal{C}_{adapt}$, modeling and simulation was done using the HIL real-time support, while the transition from the model to $\mathcal{C}_{adapt}$ implementation on top of nanoRK RTOS was done manually (although code generation tools for such models exist, e.g., [25]). Each of the controllers was tested on Parkinsonian BGM with $n = 10$ neurons per BG region.

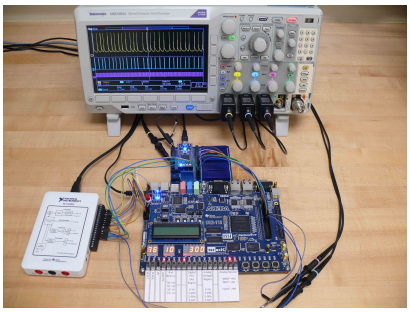

Figure 12. Experimental setup for DBS controller evaluation, supporting HIL simulation of controller models as well as testing of physical devices.

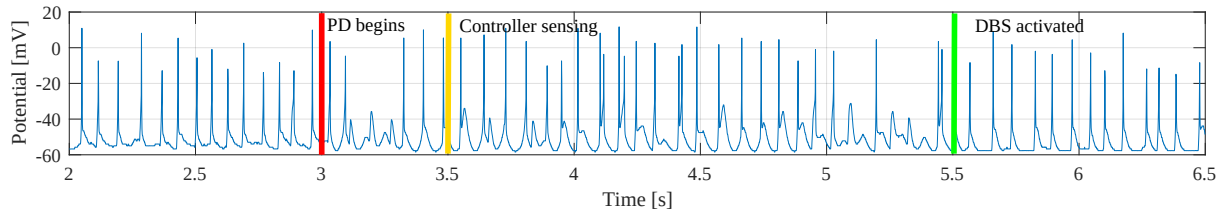

Figure 13. Experimental data obtained from TH during the testing of Adaptive controller. The used BGM captured healthy behavior $3s$ into the recording, after which we switched a PD configuration on. Controller started sensing at $3.5s$, and upon detecting power increase in β band, the controller activates DBS at $5.5s$. During the time period between the onset of PD and the start of DBS, aberrant behavior such as double and missed activations can be observed. After the controllers start the stimuli, these effects vanish completely.

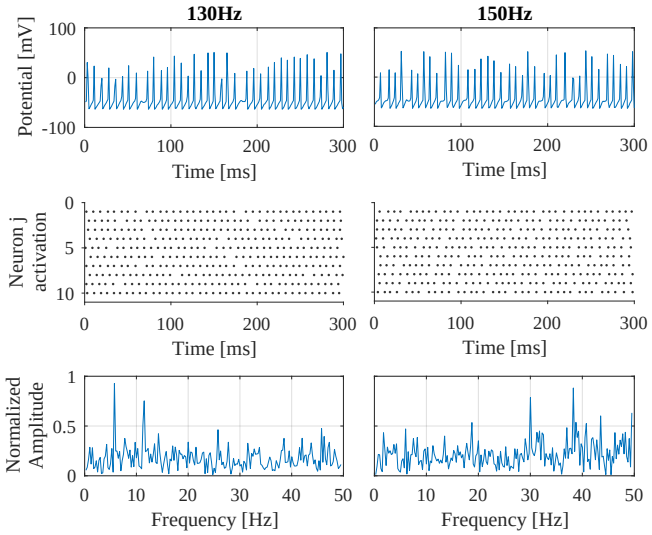

Figure 14. Effects of DBS on PD given different frequencies. Although GPi shows periodic behavior, there are no pulse trains observed for PD condition in Fig. 9. Furthermore, the β frequency band (13-35Hz) is not pronounced, showing alleviation of PD symptoms.

	Healthy	PD
EI	[0 , 0.037]	[0.1481 , 0.52]
P_β	[7.168 , 20.35]	[85.05 , 106.8]

Table III
COMPARISON OF AVERAGE QOC VALUES FOR HEALTHY BG AND PARKINSONIAN BG WITHOUT DBS.

The classic controller $\mathcal{C}_{freq}$ was tested for stimulation frequencies ranging from $130Hz$ to $180Hz$. To facilitate comparison with considered healthy and PD BGMs, we experimentally evaluated values for the QoC metrics when DBS was not used (Table III). Mean values for QoC metrics for all controller executions (Table IV) show the effectiveness of the controller. Also, the recordings from GPi neurons in Fig. 14 validate this – although activations seem more frequent than for a healthy brain on the left side of Fig. 9, the bursty neuronal activations (Fig. 9, right) were prevented, thus alleviating PD symptoms; this is especially true for 140Hz DBS (Table IV) that was more effective for the BGM configuration. Note that there are notable differences between the QoC values for effective DBS on a PD brain and the values when DBS was not used. Thus, the QoC monitors can be used to detect non-effective DBS controllers.

	$130Hz$	$140Hz$	$150Hz$	$160Hz$	$170Hz$	$180Hz$
EI	0.004	0	0	0.0015	0.0014	0.0026
P_β	23.8	8.816	14.97	15.28	19.7	16.8

Table IV
COMPARISON OF THE AVERAGE QOC MONITOR VALUES FOR VARIOUS STIMULI FREQUENCIES OF THE $\mathcal{C}_{freq}$ DBS FOR A PARKINSONIAN BG.

	PD + Pattern DBS
EI	0.0019
P_β	76.88

Table V
QOC PARAMETERS FOR A PARKINSONIAN BG STIMULATED BY $\mathcal{C}_{patt}$ WITH AVERAGE FIRING RATE CORRESPONDING TO 100HZ.

Furthermore, we tested the pattern controller $\mathcal{C}_{patt}$ for obtained DBS pattern where the HIL functionality and real-time feedback from QoC monitors were used for (suboptimal) parameter search. While results presented in Table V are not as impressive as for the $140Hz$ classic controller $\mathcal{C}_{freq}$, the stimulation rate is equivalent to 100Hz, significantly improving energy efficiency. Finally, the adaptive controller $\mathcal{C}_{adapt}$ was tested for $130Hz$ DBS, and given the separation of QoC parameters between healthy and PD conditions, it managed to detect all PD and healthy states throughout the run. Given that data remained consistent with values presented in Table III, we omit them here. A sample of recorded TH signal is shown in Fig. 13. This illustrates the benefits of closing the loop (even without sensing and actuation during the same time intervals), as the use of DBS is reduced when there was not need for it.

VI. CONCLUSION

We introduced a model-based design framework for deep brain stimulation (DBS). The main component of the framework is the basal ganglia model (BGM), specified as a network of hybrid automata, that captures physiologically relevant behaviors of healthy and Parkinsonian brains. Based on this representation, we developed software (in Simulink) and hardware (FPGA) BGM implementations, with the latter enabling real-time model simulation and device testing. The BGM was validated using a set of formal requirements that we developed, and used for design and test of three types of DBS controllers with varying levels of adaptation/feedback. To evaluate the controllers, we introduce formal Quality-of-Control (QoC) metrics and requirements that can be used for runtime monitoring of DBS effectiveness.

The BGM platform opens new opportunities to advance

DBS devices and controllers. While the BGM allows modeling varying levels of PD, our goal is to provide methods to fit BGM parameters to patient-obtained data. These patient-specific BGMs will provide clinicians a better starting set for patient-specific parameter tuning. We will also focus on developing auto-tuning and closed-loop controllers. Furthermore, different neuron configurations can be used to fit specific conditions, or even changed in real time to simulate drug effects. Finally, the BGM is a network of subsystems communicating through discrete events. This enables the use of invariant mining to generate abstraction of the model, which allows for formal controller synthesis and verification.

REFERENCES

[1] L. M. De Lau and M. M. Breteler, "Epidemiology of parkinson's disease," *The Lancet Neurology*, vol. 5, no. 6, pp. 525–535, 2006.

[2] Parkinson's Disease Foundation, "Statistics on parkinson's," 2017.

[3] D. T. Brocker, B. D. Swan, R. Q. So, D. A. Turner, R. E. Gross, and W. M. Grill, "Optimized temporal pattern of brain stimulation designed by computational evolution," *Science trans. med.*, vol. 9, no. 371, 2017.

[4] S. Little *et al.*, "Bilateral adaptive deep brain stimulation is effective in parkinson's disease," *J Neurol Neurosurg Psychiatry*, p. jnnp, 2015.

[5] A. A. Kühn *et al.*, "High-frequency stimulation of the subthalamic nucleus suppresses oscillatory β activity in patients with parkinson's disease in parallel with improvement in motor performance," *Journal of Neuroscience*, vol. 28, no. 24, pp. 6165–6173, 2008.

[6] Z. Jiang, M. Pajic, and R. Mangharam, "Cyber-Physical Modeling of Implantable Cardiac Medical Devices," *Proceedings of the IEEE*, vol. 100, no. 1, pp. 122–137, Jan 2012.

[7] FDA, "Class 2 Device Recall Activa PC, Activa RC, Active SC, https://www.accessdata.fda.gov/SCRIPTs/cdrh/cfdocs/cfres/res.cfm?id=122514," 2013.

[8] D. Selwood, "Software that can kill," *EE Journal*, 2012.

[9] Q. Stewart and K. Fu, "A second look: Analysis of FDA recalls of software-based medical devices," 2010.

[10] I. Lee, *et al.*, "Challenges and research directions in medical cyber-physical systems," *Proc. of the IEEE*, vol. 100, no. 1, pp. 75–90, 2012.

[11] J. E. Rubin and D. Terman, "High frequency stimulation of the subthalamic nucleus eliminates pathological thalamic rhythmicity in a computational model," *Journal of computational neuroscience*, vol. 16, no. 3, pp. 211–235, 2004.

[12] R. Q. So, A. R. Kent, and W. M. Grill, "Relative contributions of local cell and passing fiber activation and silencing to changes in thalamic fidelity during deep brain stimulation and lesioning: a computational modeling study," *Journal of computational neuroscience*, vol. 32, no. 3, pp. 499–519, 2012.

[13] D. Terman, J. E. Rubin, A. Yew, and C. Wilson, "Activity patterns in a model for the subthalamopallidal network of the basal ganglia," *Journal of Neuroscience*, vol. 22, no. 7, pp. 2963–2976, 2002.

[14] K. Kumaravelu, D. T. Brocker, and W. M. Grill, "A biophysical model of the cortex-basal ganglia-thalamus network in the 6-ohda lesioned rat model of parkinson's disease," *Journal of computational neuroscience*, vol. 40, no. 2, pp. 207–229, 2016.

[15] B. Colder, "The basal ganglia select the expected sensory input for predictive coding. https://commons.wikimedia.org/wiki/File:Cortical_surface_with_an_overlay_of_the_basal_ganglia_and_thalamus.jpg," 2015.

[16] A. M. Kuncel and W. M. Grill, "Selection of stimulus parameters for deep brain stimulation," *Clinical neurophysiology*, vol. 115, no. 11, pp. 2431–2441, 2004.

[17] M. Okun S. and P. Zeilman R., "Parkinson's disease: Guide to deep brain stimulation therapy, http://www.parkinson.org/sites/default/files/Guide_to_DBS_Stimulation_Therapy.pdf."

[18] S. Stanslaski *et al.*, "Design and validation of a fully implantable, chronic, closed-loop neuromodulation device with concurrent sensing and stimulation," *IEEE Transactions on Neural Systems and Rehabilitation Engineering*, vol. 20, no. 4, pp. 410–421, 2012.

[19] C. Pena *et al.*, "An overview of fda medical device regulation as it relates to deep brain stimulation devices," *IEEE Trans. on Neural Systems and Rehabilitation Engineering*, vol. 15, no. 3, pp. 421–424, 2007.

[20] A. L. Hodgkin and A. F. Huxley, "A quantitative description of membrane current and its application to conduction and excitation in nerve," *The Journal of physiology*, vol. 117, no. 4, pp. 500–544, 1952.

[21] R. Alur, F. Ivancic, J. Kim, I. Lee, and O. Sokolsky, "Generating embedded software from hierarchical hybrid models," in *Proceedings of the 2003 ACM SIGPLAN Conference on Language, Compiler, and Tool for Embedded Systems*, ser. LCTES '03, 2003, pp. 171–182.

[22] N. Mallet *et al.*, "Parkinsonian beta oscillations in the external globus pallidus and their relationship with subthalamic nucleus activity," *Journal of neuroscience*, vol. 28, no. 52, pp. 14 245–14 258, 2008.

[23] H. Bergman, T. Wichmann, B. Karmon, and M. DeLong, "The primate subthalamic nucleus. ii. neuronal activity in the mptp model of parkinsonism," *Journal of neurophysiology*, vol. 72, no. 2, pp. 507–520, 1994.

[24] D. Ruskin, D. Bergstrom, and J. Walters, "Nigrostriatal lesion and dopamine agonists affect firing patterns of rodent entopeduncular nucleus neurons," *J of neurophysiology*, vol. 88, no. 1, pp. 487–496, 2002.

[25] M. Pajic, Z. Jiang, I. Lee, O. Sokolsky, and R. Mangharam, "Safety-critical Medical Device Development Using the UPP2SF Model Translation Tool," *ACM Trans Embed Comp Syst*, vol. 13, pp. 1–26, 2014.

APPENDIX
DETAILED DYNAMICS OF THE BASAL GANGLIA MODEL

To help with brevity of equations for the model from [12], we will sometimes use v rather than $v^r,\ r \in \{STN, TH, GPi, GPe\}$ when there is no confusion.

Thalamus (TH):

$$C_m \dot{v}^{TH} = i^{TH}_{phys}(v^{TH}) + i_{SMC} - i_{GPi \to TH}$$
$$i^{TH}_{phys}(v) = -i_L - i_{Na} - i_K - i_T$$
$$\dot{h} = (h_\infty - h)/\tau_h(v)$$
$$\dot{r} = (r_\infty - r)/\tau_r(v)$$

where

$$i_L = g_L(v - E_L);\ g_L = 0.05$$
$$i_{Na} = g_{Na} m_\infty(v)^3 h (v - E_{Na})$$
$$m_\infty(v) = 1/(1 + exp(-(v+37)/7))$$

$$
\begin{aligned}
h_\infty(v) &= 1/(1+\exp((v+41)/4)) \\
\tau_h(v) &= \frac{1}{0.128\exp\left(-\frac{v+46}{18}\right)+4/\left(1+\exp\left(-\frac{v+23}{5}\right)\right)} \\
g_{Na} &= 3; E_{Na} = 50 \\
i_K &= g_K(0.75(1-h))^4(v-E_K) \\
g_K &= 5;\ E_K = -75 \\
i_T &= g_T p_\infty(v)^2 r(v-E_T) \\
p_\infty(v) &= 1/(1+\exp(-(v+60)/6.2)) \\
r_\infty(v) &= 1/(1+\exp((v+84)/4)) \\
\tau_r(v) &= 0.15(28+\exp(-(v+25)/10.5)) \\
g_T &= 5;\ E_T = 0
\end{aligned}
$$

Subthalamic Nucleus (STN):

$$
\begin{aligned}
C_m\dot{v}^{STN} &= i^{STN}_{phys}(v^{STN}) + I^{STN}_{app} + i_{dbs} - i_{GPe\to STN} \\
i^{STN}_{phys}(v) &= -i_L - i_{Na} - i_K - i_T - i_{Ca} - i_{ahp} \\
\dot{h} &= 0.75(h_\infty - h)/\tau_h(v) \\
\dot{n} &= 0.75(n_\infty - n)/\tau_n(v) \\
\dot{r} &= 0.2(r_\infty - r)/\tau_r(v) \\
\dot{c} &= 0.08(c_\infty - c)/\tau_c(v) \\
\dot{CA} &= 3.75\cdot 10^{-5}(-I_{Ca} - I_T - 22.5CA)
\end{aligned}
$$

where

$$
\begin{aligned}
i_L &= g_L(v-E_L);\ g_L = 2.25;\ E_L = -60 \\
i_{Na} &= g_{Na} m_\infty(v)^3 h(v-E_{Na}) \\
m_\infty(v) &= 1/(1+\exp(-(v+30)/15)) \\
h_\infty(v) &= 1/(1+\exp((v+39)/3.1)) \\
\tau_h(v) &= 1+500/(1+\exp((v+57)/3)) \\
g_{Na} &= 37;\ E_{Na} = 55 \\
i_K &= g_K n^4(v-E_K);\ g_K = 45;\ E_K = -80 \\
n_\infty(v) &= 1/(1+\exp(-(v+32)/8)) \\
t_n(v) &= 1+100/(1+\exp((v+80)/26)) \\
i_T &= g_T a_\infty(v)^3 b_\infty(r)^2 r(v-E_T) \\
a_\infty(v) &= 1/(1+\exp(-(v+63)/7.8)) \\
b_\infty(r) &= 1/\left(1+\exp\left(-\frac{r-0.4}{0.1}\right)\right) - 1/(1+\exp(4)) \\
r_\infty(v) &= 1/(1+\exp((v+67)/2)) \\
t_r(v) &= 7.1+17.5/(1+\exp((v+68)/2.2)) \\
g_T &= 0.5;\ E_T = 0 \\
i_{Ca} &= g_{Ca} c^2(v-E_{Ca}) \\
c_\infty(v) &= 1/(1+\exp(-(v+20)/8)) \\
t_c(v) &= 1+10/(1+\exp((v+80)/26)) \\
g_{Ca} &= 2;\ E_{Ca} = 140 \\
i_{ahp} &= g_{ahp}(v-E_{ahp})(CA/(CA+15)) \\
g_{ahp} &= 20;\ E_{ahp} = -80
\end{aligned}
$$

Globus Pallidus (Both GPi and GPe):

$$
\begin{aligned}
C_m\dot{v}^{GP} &= i^{GP}_{phys}(v^{GP}) + I^{GP}_{app} - i_{STN\to GP} - i_{GPe\to GP} \\
i^{GP}_{phys}(v) &= -i_L - i_{Na} - i_K - i_T - i_{Ca} - i_{ahp} \\
\dot{h} &= 0.75(h_\infty - h)/\tau_h(v) \\
\dot{n} &= 0.75(n_\infty - n)/\tau_n(v) \\
\dot{r} &= 0.2(r_\infty - r)/\tau_r(v) \\
\dot{CA} &= 1\cdot 10^{-4}(-I_{Ca} - I_T - 15CA)
\end{aligned}
$$

where

$$
\begin{aligned}
i_L &= g_L(v-E_L);\ g_L = 0.1;\ E_L = -65 \\
i_{Na} &= g_{Na} m_\infty(v)^3 h(v-E_{Na}) \\
m_\infty(v) &= 1/(1+\exp(-(v+37)/10)) \\
h_\infty(v) &= 1/(1+\exp((v+58)/12)) \\
\tau_h(v) &= 0.05+0.27/(1+\exp((v+40)/12)) \\
g_{Na} &= 120;\ E_{Na} = 55 \\
i_K &= g_K n^4(v-E_K) \\
n_\infty(v) &= 1/(1+\exp(-(v+50)/14)) \\
\tau_n(v) &= 0.05+0.27/(1+\exp((v+40)/12)) \\
g_K &= 30;\ E_K = -80 \\
i_T &= g_T a_\infty(v)^3 r(v-E_T) \\
a_\infty(v) &= 1/(1+\exp(-(v+57)/2)) \\
r_\infty(v) &= 1/(1+\exp((v+70)/2)) \\
g_T &= 0.5;\ E_T = 0 \\
i_{Ca} &= g_{Ca} s_\infty(v)^3(v-E_{Ca}) \\
s_\infty(v) &= 1/(1+\exp(-(v+35)/2)) \\
g_{Ca} &= 0.15;\ E_{Ca} = 120 \\
i_{ahp} &= g_{ahp}(v-E_{ahp})(CA/(CA+10)) \\
g_{ahp} &= 10;\ E_{ahp} = -80
\end{aligned}
$$

Synaptic functions parameters:

Synapses	Parameters	
$i_{STN\to GPe}$	$g_{syn} = 0.15$	$E_{syn} = 0$
$i_{STN\to GPi}$	$g_{syn} = 0.15$	$E_{syn} = 0$
$i_{GPe\to STN}$	$g_{syn} = 0.5$	$E_{syn} = -85$
$i_{GPe\to GPe}$	$g_{syn} = 0.5$	$E_{syn} = -85$
$i_{GPe\to GPi}$	$g_{syn} = 0.5$	$E_{syn} = -85$
$i_{GPi\to TH}$	$g_{syn} = 0.17$	$E_{syn} = -85$

Modeling Healthy and Parkinsonian condition:

Previously defined model can capture both healthy and PD conditions of BG. The change between the two is possible through proper selection of the I_{app} current.

Conditions	I^{STN}_{app}	I^{GPe}_{app}	I^{GPi}_{app}
Healthy	$33\mu A/cm^2$	$20\mu A/cm^2$	$21\mu A/cm^2$
Parkinsonian	$23\mu A/cm^2$	$7\mu A/cm^2$	$15\mu A/cm^2$